PHOTONICS Research

2D-material-integrated whispering-gallery-mode microcavity

Lu Wang, Xuefei Zhou, Shuo Yang, Gaoshan Huang, and Yongfeng Mei*

Department of Materials Science and State Key Laboratory of ASIC and System, Fudan University, Shanghai 200433, China
**Corresponding author: yfm@fudan.edu.cn*

Received 16 May 2019; revised 23 June 2019; accepted 25 June 2019; posted 25 June 2019 (Doc. ID 367320); published 26 July 2019

Optical microcavities, which support whispering gallery modes, have attracted tremendous attention in both fundamental research and potential applications. The emerging of two-dimensional materials offers a feasible solution to improve the performance of traditional microcavity-based optical devices. Besides, the integration of two-dimensional materials with microcavities will benefit the research of heterogeneous materials on novel devices in photonics and optoelectronics, which is dominated by the strongly enhanced light–matter interaction. This review focuses on the research of heterogeneous two-dimensional-material whispering-gallery-mode microcavities, opening a myriad of lab-on-chip applications, such as optomechanics, quantum photonics, comb generation, and low-threshold microlasing.

https://doi.org/10.1364/PRJ.7.000905

1. INTRODUCTION

Optical microcavities, which can confine light by resonant recirculation, have offered great opportunities and challenges in both fundamental research and practical applications in the past decades [1–3]. Among all kinds of optical microcavities, whispering gallery mode (WGM) microcavities derived from typically dielectric spherical structures have attracted interest in the fields of lasers, filters, sensors, optical diodes, and comb generation for their high quality factor (Q factor), small volume, and easy integration [4–8].

In a WGM microcavity, waves propagate and accumulate along the surface of the microcavity by continuous total reflection [9]. Microcavities with diverse geometrical features have been proposed and demonstrated. Microspheres, which have typically attracted considerable attention, can support an ultrahigh Q factor due to their excellent surface smoothness [10]. Microcapillaries have the advantage in the fabrication process and sensing performance based on their hollow structures [11]. Similarly, microbottles are fabricated from silica microcapillaries by a pressure-compensated method for three-dimensional (3D) confinement of resonant modes [12]. Microring, microdisk, and microtoroid cavities provide platforms for the on-chip integration with devices, in the meanwhile, support high-Q factors [13,14]. While the output of WGM resonators based on microrings, microdisks, and microtoroids is in the parallel dimension with respect to the chip panel, rolled-up microtubular resonators offer an approach to achieve vertically emitting modes with easy integration and large-area fabrication [15–17]. Furthermore, based on the rolled-up technology, microtubes with a bottle-like geometry have been explored and attracted intense attention for their precisely controlled axial modes and highly enhanced Q factors [18]. Recently, a single-mode confinement-enhanced tubular microcavity was constructed by rolling up diamond nanomembranes, in which periodic hole arrays along the circumference were precisely engineered to realize discrete rotational symmetry [19]. So far, the geometrical innovation of WGM microcavities has led to remarkable development in both fundamental research and practical applications.

In addition, materials selected to construct a microcavity are not limited to silica or silicon, as a variety of materials have shown extensively excellent properties and corresponding application potentials, e.g., ZnO, $LiNbO_3$, diamond, polymer, and high-refractive-index oxides (Y_2O_3 and ZrO_2) [20–24]. In the meanwhile, the recent and intensive development in two-dimensional (2D) materials gives birth to a new focus on exceptional photonic performance for the strong interaction between light and many 2D materials [25]. Most importantly, 2D materials can be integrated into functional photonic devices and systems, enabling unique devices and applications with high performances. First, the 2D-material-enabled modification of WGMs offers a potential solution to much richer physical properties, such as tunable light sources [26]. Owing to the effect arising from small size, low-dimensional materials provide intriguing opportunities for nanostructure-dependent properties and related photonic performances as compared with their bulk counterparts [27]. In particular, 2D materials present a better-defined interface geometry for quantitative characterization than 0D and 1D materials, allowing novel devices based on the junction interface, e.g., gate-tunable properties [28]. Second, it is of great significance for the integration of 2D

materials on microcavities, realizing enhanced light–matter interaction [29]. Thus, 2D-material-coupled WGM microcavities have stimulated intensive research and enormous progress in fundamental physics and future perspectives.

In this review, we will discuss the development of 2D-material-coupled WGM microcavities, with examples of scientific research and applications in different kinds of microcavities like microdisks, microspheres, and microtoroids. Starting with the graphene-integrated microcavity, we will mainly focus on the plasmonic hybrid mode and explore its superior property in sensitivity and tunability. For transition metal dichalcogenides (TMDCs), they have attracted growing interest due to their distinct features in high optical gain. We will present a discussion on the development of 2D materials among WS_2, WSe_2, and MoS_2, where the appealing phenomena of excitonic lasing and spontaneous emission enhancement arise. Moreover, other kinds of emerging 2D materials and coupling schemes will also be discussed for their feasibility and future perspectives, such as black phosphorus and hexagonal boron nitride (hBN). Additionally, the integration of 2D materials based on the rolled-up technique is proposed, which would endow such a heterogeneous material microcavity with a novel coupling scheme and possible potentials in on-chip devices. The 2D material-coupled microcavities will offer promising scientific discoveries and nanophotonics technologies for future devices.

2. GRAPHENE-INTEGRATED WGM MICROCAVITY

Graphene, as one kind of atomically thin material, has arisen intense interest due to its extraordinary properties in both electronics and photonics [30,31]. Compared with traditional materials in bulk form, graphene exhibits a variety of appealing phenomena, which arises from its dissimilar band structure near the Fermi level [32–35]. It is demonstrated that the ultrahigh mobility of graphene can support the study of ultrafast optoelectronic devices, such as modulators and photodetectors [36,37]. Besides, graphene interacts with light from microwave to ultraviolet wavelengths, which indicates its adaptability towards different applications owing to the broadband response [38]. It is worth noting that the tunability of a graphene-based device can be easily realized, where Fermi levels and corresponding properties can be tuned towards target applications [39–41]. Technically, the small size and easy integration with complementary metal oxide semiconductor (CMOS) techniques enable graphene the next-generation devices in both on-chip and flexible strategies. Based on the integration of graphene on a photonic crystal nanocavity, a strong enhancement in light–matter interaction has been realized, which opens the door to novel optical devices including hybrid systems for sensitivity improvement [42,43].

A. High Sensitivity

In early studies, graphene is demonstrated to support both localized and propagating plasmons, which is concluded as one of its semimetallic features [44,45]. Compared with plasmons in metals, graphene plasmons cover the region from terahertz to the midinfrared wavelengths. Besides, the plasmonic nanostructures based on noble metals suffer from high adsorption loss and low damage threshold, which limit conversion efficiency and hinder practical applications. Thus, the research on hybrid plasmonic modes in the WGM microcavity is restricted until the introduction of graphene as an optimal choice, enabling devices with high performances, such as ultrahigh sensitivity.

Based on a graphene-coated microcavity, surface plasmon polaritons propagate along the surface and interact with the whispering gallery waves, thus realizing the hybrid plasmonic modes. So far, calculations and simulations have been performed to reveal the mechanism and effects. In general, the periodic boundary condition and effective thickness are often applied to raise the efficiency and ensure the accuracy when dealing with atomically thin 2D materials [46]. Typically, the dynamical conductivity of graphene can be determined from the Kubo formula, which is further utilized for the optical constants as a function of chemical potential and wavelength [47]. Figure 1(a) exhibits the 5 nm radius InGaAs nanowire cavity coated with graphene [48]. In such a nanoscale configuration, the plasmonic waves are tightly confined on the interface between graphene and the free space, as demonstrated in the electromagnetic field distribution from the inset of Fig. 1(a). In addition, it is of great significance to note that the surface conductivity would strongly affect the resultant surface plasmon polaritons. Thus, one can manipulate the hybrid plasmonic modes by controlling the chemical potential through a myriad of methods, e.g., doping, gating, and strain engineering [39–41]. The researchers also theoretically conclude the Q factor and mode number as functions of the chemical potential [48]. As depicted in Fig. 1(b), the increase of chemical potential leads to the decrease in propagation loss of the plasmonic modes and the enhancement in the Q factor. The ultrasmall mode volume suggests the plasmonic WGM microcavity as a promising candidate for label-free sensors [48]. Besides, a graphene-based THz ring microcavity was proposed for sensing with label free and lab-on-a-chip features [49]. The multilayered microcavity consists of a dielectric layer Si_3N_4, a buffer layer SiO_2, a graphene layer, and a porous cladding layer p–Al_2O_3. The performance of the hybrid microcavity is characterized through the fiber-coupling technique, where the light transmission shows a dip at the resonance wavelength. The refractive index of the cladding layer changes with adsorption of target molecules. Thus, the resonance wavelength shifts correspondingly, which consequently can be utilized for molecule detection. The authors also reveal the relationship between the resonance wavelength shift and the refractive index change of the cladding layer for different chemical potentials of graphene [49]. The decrease of chemical potential helps to enhance the sensitivity, which is dominated by better confinement of the surface plasmon mode. The sensitivity of the proposed configuration is calculated to be 46 μm/RIU, which indicates a 30-time enhancement compared with that of a whole dielectric structure. For the application potentials in integrated photonics, a graphene-sandwiched silica microdisk is proposed, as shown in Fig. 1(c), where the tunability of sensitivity is realized by electrically adjusting the permittivity of graphene [50]. Particularly, when the permittivity is around the epsilon-near-zero point, there would be a distinct change in the sensitivity, as shown

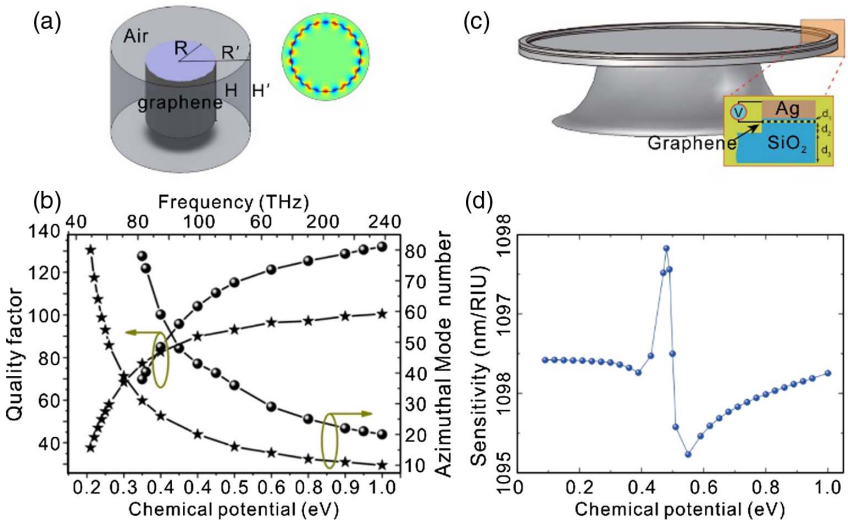

Fig. 1. (a) Schematic of the graphene (dark grey) coated nanodisk (light blue) and the corresponding Comsol finite element computational window (light gray). Inset is the horizontal view of the electric field distribution [48]. (b) Q factor and azimuthal mode number as functions of the chemical potential corresponding to 63.2 and 89.4 THz [48]. (c) Schematic of graphene-integrated microdisk cavity [50]. (d) Sensitivity as a function of the chemical potential [50].

in Fig. 1(d), which reveals its potential applications in devices with high modulation depth and high sensitivity. However, the Q factors of graphene-coated microcavities are still poor compared with those of traditional dielectric microcavities. In order to alleviate the loss for high Q factors, it is proposed that one can effectively utilize a vertically coupled monolayer graphene microcavity, via keeping their distance instead of straight contact [51].

Except for the sensing mechanism based on the refractive index change of the surrounding environment, it also attracted intense attention by monitoring the refractive index change of graphene based on its environment-sensitive conductivity [52]. When exposed to target gas, the C-C bonds would be modified with gas molecules; thus, the carrier concentration is tuned [53]. The complex refractive index, which is dependent on graphene's conductivity, is sensitive to the change of the surrounding gas concentration [54]. Additionally, graphene and one of its derivate graphene oxides (GOs) are ideal materials for biomolecules and gas molecule adsorption for the large specific surface area and high adsorption [55]. So far, there are various methods employed in gas sensing based on graphene and GOs [56,57]. The sensing scheme based on optical microcavities indicates its advantages in high sensitivity and real-time detection. Figure 2(a) depicts the configuration of a GO-coated ring microcavity [54]. The authors monitored the shift of the resonant wavelength in transmission spectra, which is illustrated in Fig. 2(b) for the NH_3 gas with concentrations of 0, 75, 150, 225, and 300 ppm (parts per million). Additionally, the sensitivities of NH_3 and CO are different due to the adsorption energy and charge transfer ability, which indicates the potential applications in differentiating gas [58].

Furthermore, the novel sensing mechanism based on an optomechanical microcavity is demonstrated, which enables a graphene-based ultrasensitive gas detection [59]. Figure 2(c) depicts the schematic of the graphene-enhanced Brillouin microcavity, where a layer of GO film is deposited on the inner wall of the microbottle. Once the NH_3 gas is introduced to the microbottle cavity with a concentration of 10 ppm, the beat note shifts from 262.0 to 260.4 MHz, which is monitored on the Brillouin and acoustic mechanical scattering. Such a hybrid microcavity enables extremely high sensitivity up to 200 kHz/ppm based on the novel "electron–phonon–photon" process. This phenomenon reveals the synergy effect of graphene and microcavity for enhanced sensitivity and ultrafast response, which hints that the combination of graphene can broaden the potential applications in sensing [60,61].

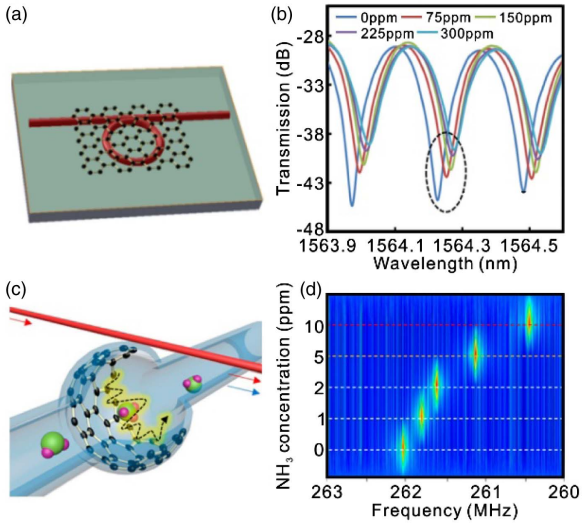

Fig. 2. (a) Schematic of the graphene-oxide-coated microring resonator [58]. (b) Transmission spectra under different concentrations of NH_3 gas [58]. (c) Conceptual design of a graphene-oxide-layer-incorporated silica capillary resonator [59]. (d) Colored map of the beat note spectra under different concentrations of NH_3 gas [59].

B. Tunability

Graphene has attracted increasing attention as a promising tunable material thanks to the great potential in manipulating the Fermi level and carrier concentration [62]. While the existing microcavities suffer from a lack of tunability due to the fixed geometries and large bandgaps of constituent materials, it has become the first priority to be settled to realize the application in the fields of photonics engineering. Thus, the incorporation of graphene in microcavities is worth consideration and discussion.

Since the development of telecommunications and optical interconnections, it demands for optical modulators with exceptional performance, where ring modulators based on WGMs were successively developed with small dimensions, power consumption, and broadband response. Still, the narrow bandwidth that microcavities support limits their further applications. Since a graphene-based optical modulator has attracted strong attention, it was proposed that a novel graphene-integrated microring modulator was promising in featuring a large bandwidth through numerical simulations [63,64]. In 2015, the first graphene microring modulator was fabricated based on the leveraging critical coupling effects [65]. As depicted in Fig. 3(a), the integrated capacitor was used to modulate the loss of WGMs through the Fermi-level-dependent adsorption in graphene sheets [65]. By increasing the voltage, the absorption would be decreased, thus enabling the change from the undercoupled to critical coupled state. The modulation depth is over 15 dB with 10 V, as shown in Fig. 3(b), indicating the increased speed and efficiency using a graphene-integrated microring modulator. Since then, effective modulation has been achieved in a heterogeneous graphene microring with a high modulation depth, broadband response, ultrafast operation speed, and small footprint [66].

Moreover, considering the high value of graphene's thermal conductivity, a thermo-optic microring modulator was demonstrated for an effective modulation featured with a small footprint [67]. As depicted in Fig. 3(c), the authors have transferred monolayer graphene on a microring resonator, where Joule heating was produced by electrodes. Once the heat is transferred onto the microring, there would be a change in the refractive index, thus enabling the modulation. As shown in Fig. 3(d), by applying an increasing voltage, there would be a redshift in the resonant wavelength and a decrease in the transmission drop, realizing "OFF" to "ON" state of the hybrid modulator. Further, thermo-optic all-optical devices based on the graphene-integrated microring modulator have been investigated, where the all-optical processing has advantages in power efficiency since the conversion between optical and electronic signals was no longer necessary [68–70]. Thus, a graphene-microcavity modulator is demonstrated as an efficient device based on mechanisms among electro-optic, electrorefractive, and thermo-optic, promising an ideal platform for applications [71–74].

As the tunable optical constants have been realized in the graphene heterogeneous microcavity, it can be applied in functional devices that depend on a specific relation between optical constants and resonances. Thus, the analog of electromagnetically induced transparency has been demonstrated with electrical control, showing great potential in light transmission for quantum information technology [75]. Additionally, the structure of the graphene-based microring was integrated with a source drain and top gating, as shown in Fig. 3(e), which enables a tunable-frequency Kerr comb by altering the Fermi level of graphene through gate tuning [76]. Figure 3(f) gives the primary comb lines under different gate voltages. For applied voltages of −1, −1.2, and −1.5 V, the frequency offsets are observed at 2.36, 3.25, and 7.17 THz, respectively, while for the applied voltage up to −1.8 V, there is no longer a frequency comb since it became harder for phase matching. Based on the gate-tunable primary comb, a series of phenomena is realized including coherent Kerr frequency combs, controllable Cherenkov radiation, and soliton states [77]. The electrically dynamic control of diverse comb outputs could enable the application of optical frequency combs in precision measurements and optical signal processing. Briefly, the remarkable tunability has made graphene a promising heterogeneous material for

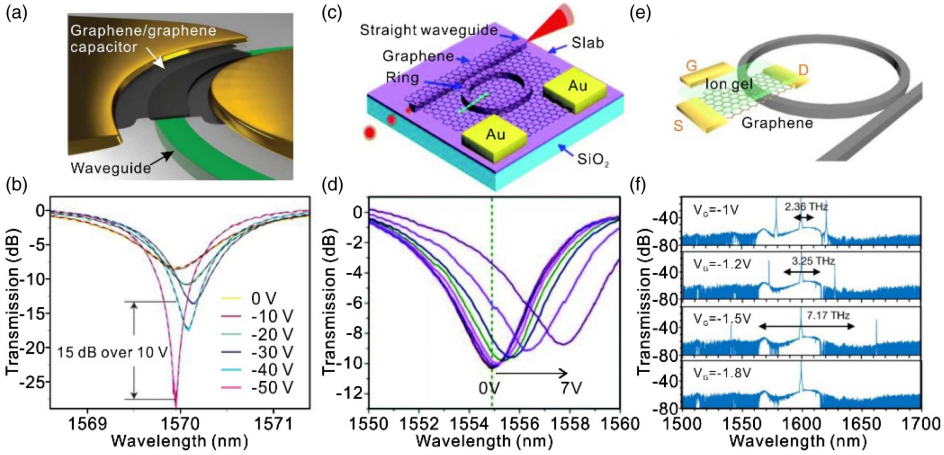

Fig. 3. (a) Schematic of the modulator based on a graphene/graphene capacitor integrated with a microring cavity [65]. (b) Transmission spectra and theoretical results as a function of dc voltages [65]. (c) Schematic of the modulator based on a graphene-integrated microring cavity [67]. (d) Transmission spectra under different drive voltages [67]. (e) Schematic of the integration of a graphene/ion-gel heterostructure on a microring cavity [76]. (f) Primary comb lines at different gate voltages [76].

integration with microcavities as optical devices with high performance in fundamental researches and future applications of superior response speed and operation bandwidth.

C. Lasing Performance

Graphene surface plasma could be applied to transport and manipulate photons, which may confine the optical field and strengthen the light–matter interaction, leading to the spontaneous emission. ZnO, with wide direct bandgap (3.37 eV) and strong exciton binding energy (60 meV), has drawn intense attention in the research of short-wavelength lasers [78]. So far, different kinds of resonant cavities have been employed in ultraviolet lasing of ZnO, and WGM microcavities have excellent performance owing to their small volume, high Q factor, and low lasing threshold [79,80]. To further improve the spontaneous and stimulated emission, microcavities based on a monolayer graphene-coated ZnO microrod with hybrid modes are proposed. Graphene plasmon could help the near-field coupling in the ultraviolet range of ZnO emission, thus leading to optical confinement and lasing enhancement [81]. As shown in Fig. 4, the lasing intensity of graphene-coated ZnO microrods is significantly improved, which is dominated by the coupling between the graphene surface plasmon and the ZnO exciton emission [81]. It could be further validated through the optical images in Fig. 4, which demonstrated that a graphene/ZnO hybrid submicron microcavity can effectively confine the optical field and enhance the optical gain [82]. Afterwards, researchers have theoretically and experimentally investigated the lasing performance based on graphene/ZnO microcavities with the reduced lasing threshold, the increased Q factor, and the enhanced lasing peak intensity [82], which inspired research in low-threshold lasers using micro/nanostructures.

Additionally, the crystalline graphene layer could be employed as a nucleation layer to grow high-quality microrods via epitaxial growth. As for lasing applications, gallium nitride (GaN) microdisks have been prepared, realizing WGM lasing at room temperature [83]. Also, it is demonstrated that the GaN microstructures could serve as bendable light-emitting diode (LED) arrays, offering possibilities in the field of large-scale and flexible optoelectronic devices [84]. Besides, single-crystalline organic nanowires could also grow vertically on the surface of graphene, working as efficient optical waveguides and forming resonances [85]. Moreover, electrically driven nanolasers using graphene as electrodes were achieved first in 2012, based on a graphene-covered microdisk [86]. Graphene is expected to offer the potential in the combination of unique electronic properties and tunable optical performances. Thus, in the research of nanolasers based on single-crystalline microcavities, graphene not only helps with the epitaxy growth in a simple procedure, but also provides effective optical confinement and electric injection, realizing future on-chip light sources.

3. TMDCS-INTEGRATED WGM MICROCAVITY

While graphene is gapless and semimetallic, TMDCs are semiconductors with a bandgap ranging from 1.0 to 2.0 eV that experience an indirect-to-direct bandgap transition as the number of layers is reduced to monolayer, creating new optical functionality in optoelectronics [87–91]. TMDCs offer strong light emission and high exciton binding energy due to the quantum confinement effect and reduced screening of the Coulomb force [92–95]. The outstanding optical properties make TMDCs potential materials for high-performance optoelectronics and photonics devices. However, the efficiency of a heterogeneous device is limited by the innate thickness of 2D materials, while integrating TMDCs with photonics structures, such as a microcavity and photonic crystal, offers a solution to enhance light–matter interaction. Thus, the coupling would benefit the research on excitonic properties of monolayer TMDCs and novel devices in 2D photonics and optoelectronics [96,97]. Particularly, the integration of TMDC material with WGM microcavities could support high-quality resonance, serving as a photonic light source [98,99].

A. Exciton Emission

TMDCs are promising candidates for novel optical and optoelectronic devices, which can be attributed to their direct bandgap when the number of layers is reduced to a monolayer [92]. The strong transition between valence and conduction bands is demonstrated to be excitonic, thus providing a feasible platform for the research on optical gain and stimulated emission. Further, excitonic lasing has been observed and studied through the integration of 2D TMDCs and optical microcavities, which allows for the significant enhancement on the interaction between the gain medium and photon [100–103]. First, the feasibility of lasing based on TMDC-integrated cavities was demonstrated by use of a photonic cavity, which

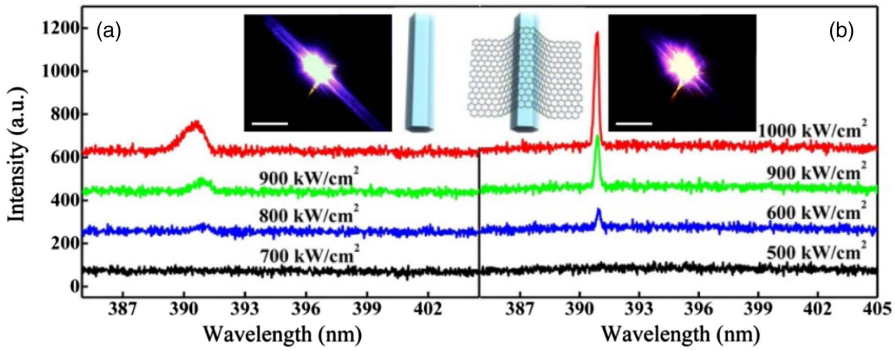

Fig. 4. PL spectra of (a) the ZnO rod and (b) the graphene-covered ZnO rod. Insets are the dark-field optical images and schematics of an individual ZnO rod before and after the cover of graphene under laser excitation. The scale bars correspond to 50 μm [81].

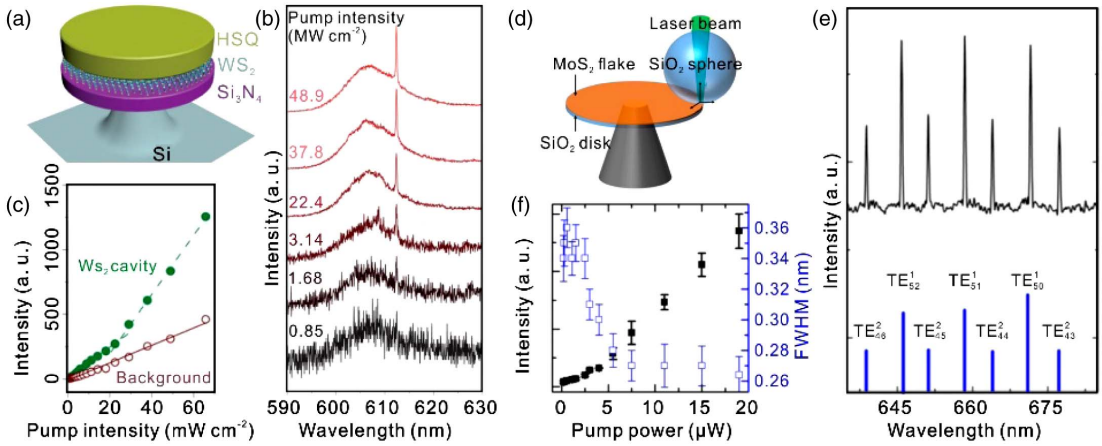

Fig. 5. (a) Schematic of a monolayer WS_2 microdisk cavity with a sandwiched structure of Si_3N_4/WS_2/HSQ [102]. (b) PL emission spectra under increasing pump intensity [102]. (c) Monolayer WS_2 PL background and cavity emissions as functions of pump intensity [102]. (d) Schematic of the coupled microsphere/microdisk cavity with the integration of MoS_2 [103]. (e) PL spectrum after subtracting the background emission (top panel) and the calculated WGM positions (bottom panel) [103]. (f) The integrated intensity and FWHM as functions of excitation power [103].

could significantly reduce the lasing threshold of the emitter, as reported in 2015 [101]. In the same year, the electromagnetic environment of the TMDC emitter was further engineered through WGM microcavities [102,103]. Ye *et al.* explored a sandwiched configuration, where the optical gain medium was embedded between two dielectric layers [Si_3N_4/WS_2/hydrogen silsesquioxane (HSQ)] with a diameter of 3.3 μm, as shown in Fig. 5(a) [102]. As the intensity of a 473 nm pump laser increases, the peak appears at 612.2 nm and increases sharply when the pump intensity is above 22.4 $mW \cdot cm^{-2}$ [Fig. 5(b)]. To clearly demonstrate the excitonic lasing behavior, the pump intensity dependence of the photoluminescence (PL) intensity is plotted for both the cavity and background PL emission in Fig. 5(c). At low pump power, the cavity emission intensity increases linearly with the excitation power. There is an abrupt increase in the curve when the pump power is above the threshold of 20 $mW \cdot cm^{-2}$, showing the evidence of excitonic lasing. A similar phenomenon was observed in the integration of a MoS_2 flake at the interface between a free-standing microdisk and microsphere with room-temperature lasing performance, as shown in Fig. 5(d) [103]. At an excitation power of 100 μW (above threshold), such a unique microcavity could support high-Q WGMs, as depicted in Fig. 5(e) with the calculated mode position in the lower panel. The intensity shows a superlinear increase and a clear linewidth narrowing when the pump power exceeds the threshold, as shown in Fig. 5(f) [103]. Additionally, the near-field coupling scheme was efficiently applied on the WSe_2-integrated microdisk, which could meet the demand in precisely measuring the excitonic emission for both in-plane and out-of-plane excitation [104]. The superior excitonic lasing performance in the visible range is attributed to the synergy effect of the large gain and the coupling between the gain medium and WGM microcavity, which effectively enhances the light–matter interaction.

B. Tunable Light Source

Typically, the interaction between a few layers of $MoTe_2$ and microring cavity has been studied, which indicates a feasible method to investigate and exploit the tunability of the coupling strength [105]. Meanwhile, the emission from TMDCs coupled to a microcavity will be influenced by many simple methods, and thus could be tuned towards the target properties. Photothermal effects are induced by photon absorption in TMDC materials when illuminated by an external light source [87,94]. The thermal effect was technically investigated by exploring a MoS_2-coupled optical microdisk cavity [106]. Figure 6(a) depicts emission spectra at different power levels. It is observed that the PL intensity reaches its maximum under illumination power of 12.3 mW and starts to decrease as the

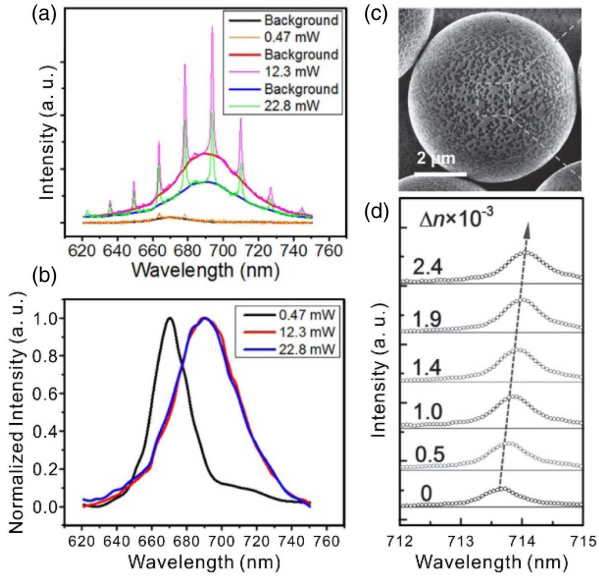

Fig. 6. (a) Emission spectra at different laser powers of 0.47, 12.3, and 22.8 mW and the corresponding background emission spectra [106]. (b) Normalized background emissions extracted from (a) [106]. (c) SEM image of the as-grown monolayer MoS_2 on SiO_2 microspheres [107]. (d) PL spectra of the main modes as a function of ethanol concentration [107].

power density extends the damage threshold since MoS_2 is permanently damaged. Background PL spectra at these three power levels were normalized, as shown in Fig. 6(b). To demonstrate the thermal effect in the MoS_2-coupled optical microdisk cavity, the PL peak position was studied, and redshifts were observed distinctively as the pump power increased from 0.47 to 12.3 mW. It is attributed to the local heating generated by nonradiative recombination processes in the MoS_2 flake, which is coincident with the peak shift phenomena of monolayer TMDC dependence on the temperature [106]. However, there is no further redshift when the pump power is above the threshold, which can be ascribed to the permanent photoinduced damage caused by thermal oxidation of the MoS_2 flakes. The result reminds researchers to avoid the thermal effect in experiments and future applications of the integrated microcavities by utilizing pulsed pump lasers to effectively minimize the heating and circumvent photothermal effects.

On the other hand, the character that emission properties could be influenced by an external factor can be exploited and applied. Mi *et al.* demonstrated the application potentials of MoS_2 microcavities in a refractive index sensor, benefiting from the shift of emission peaks [107]. In their study, a straightforward fabrication method for the integration of MoS_2 flakes and commercially available SiO_2 microsphere resonators was first explored by the chemical vapor deposition (CVD) method [107]. Figure 6(c) shows that the triangular MoS_2 flakes are uniformly distributed on the surface of SiO_2 microspheres. Compared with the transfer method in other works, the direct deposition of TMDCs provides a better contact and thus a stronger coupling. Furthermore, the size, number of layers, and coverage of MoS_2 are more controllable. The emission spectra clearly show whispering gallery resonances, which have been further validated through calculations using an explicit asymptotic formula and mode identification algorithm. The evanescent waves of WGMs are extremely sensitive to surrounding molecules, which could be monitored through the shift of the resonance peak as the refractive index varies where water serves as environment medium while certain ethanol is added to increase the refractive index. As refractive index Δn increases, resonant modes exhibit a linear redshift ($\Delta\lambda$), shown in Fig. 6(d), which demonstrates the high sensitivity of 150 nm·RIU^{-1}.

Thus, 2D-TMDC-integrated WGM microcavities have potential applications in optoelectronics devices [99,102,103,107,108]. In the future, more works should be carried out to develop a better understanding of exciton dissociation and quantum yield of the 2D materials, which will make sense to design structures and choose appropriate materials [104,109]. Van der Waals heterostructures consisting of different kinds of 2D materials exhibiting unique properties offer potential opportunities for novel photonics devices [110–113]. The integration of large-scale and high-quality bulk and monolayer samples is one of the critical tasks to improve the device performance.

4. OTHER 2D MATERIALS

Graphene and TMDCs are two kinds of 2D materials with great significances, and the study on their characteristics has created a new era. Still, there is a rising demand for research on new emerging 2D materials, e.g., black phosphorus and hBN. In 2019, the first cavity optomechanical system incorporating hBN was reported based on the WGM microdisk [114]. By positioning the hBN nanobeam in the optical near-field of a silicon microdisk, the optomechanical system is experimentally achieved and demonstrated with the observation of thermally driven mechanical resonances. Besides, the propagation of phonon polaritons in hBN potentially suggests its performance in light confinement to the deep subwavelength regime. Considering the excellent dielectric properties of hBN, a van-der-Waals-stacked hBN/WS_2/hBN formed a microdisk cavity, giving rise to emission intensity and implying the feasibility of heterogeneous-material-involved devices [111]. While black phosphorus has a direct bandgap, it can be tuned through the number of layers from 0.3 to 2.0 eV, bridging the gap between graphene and TMDCs [115–117]. The in-plane anisotropic property of black phosphorus leads to its potential in nontrivial performances, e.g., light modulating and polarization tuning [118]. Thus, the photonic properties of black phosphorus may allow its integration with microcavities for application in novel optical components of on-chip devices. Most strikingly, it is intriguing to construct photonic devices based on many kinds of heterogeneous materials comprising different bandgaps and optical properties, realizing the highly-compatible microcavity-based devices.

5. ROLLED-UP HETEROGENEOUS MATERIAL MICROTUBE AND FUTURE PERSPECTIVES

Generally, there exists detailed investigation on 2D-material-integrated microring resonators as the coupling scheme, which possess on-chip superiority and fabrication convenience [65,67,76]. However, rolled-up tubular microcavities have their typical features in structure design, fabrication, and integration, thus enabling and optimizing the coupling with heterogeneous materials [119]. The rolled-up technique has been adopted to fabricate microtubes based on prestrained nanomembranes, realizing tubular mesostructures with nanoscale wall thicknesses [20]. In the past decade, optimizations on structure design have been adopted, which effectively improved the performance of tubular microcavities. Recently, the integration of heterogeneous materials has attracted intense attention [120]. Remarkably, an 8 nm thick gold layer was deposited as a cap on top of the dielectric tubular microcavity to achieve hybridized plasmon–photon modes [121]. It was found that the selective coupling of optical WGMs and localized surface plasmons depends on the location of the nanogap, showing a strong coupling-induced mode shift. Figure 7(a) depicts the hybridized modes, which are deduced from the lobe structure, indicating the tunable magnitude of the mode shift [121]. The efficient coupling of localized surface plasmons and confined resonances in the heterogeneous material microcavity is proved to be a promising strategy for the investigation of ultrasensitive detection, polarizers, and metamaterials, where light–matter interactions are involved [122,123].

On the other hand, with the rapid development in nanoscale fabrication and demonstration, it enables the sophisticated design on the geometry of the microtube cavity. The single-mode tubular microcavity [bottom panel of Fig. 7(b)] was proposed

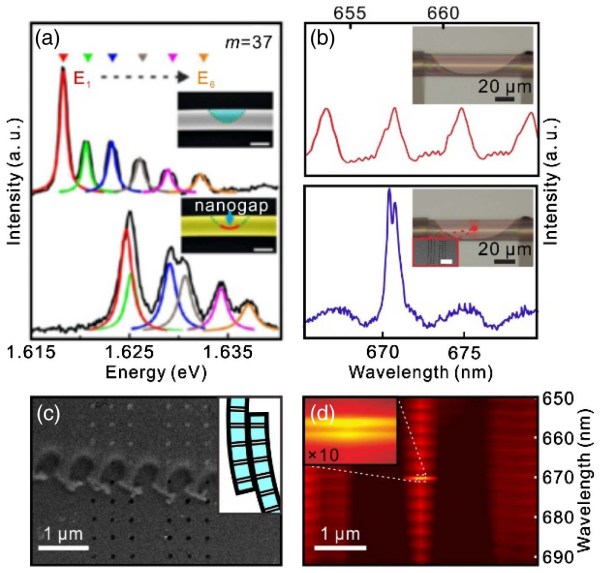

Fig. 7. (a) Axial modes measured before (top panel) and after (bottom panel) gold layer coating on rolled-up tubular microcavities with different lobe positions. Insets are morphologies of microcavities before and after gold layer coating [121]. (b) PL spectra and corresponding morphologies of the bottle-like tube (top panel) and the single-mode tube with periodic hole arrays (bottom panel) [19]. (c) SEM image of the hole array in a rolled-up diamond microcavity. Inset is the schematic of the nanomembrane cross section with patterned holes (right panel) [19]. (d) PL mapping for the rolled-up diamond microcavity. Inset is the magnified PL mapping of the confinement-enhanced mode [19].

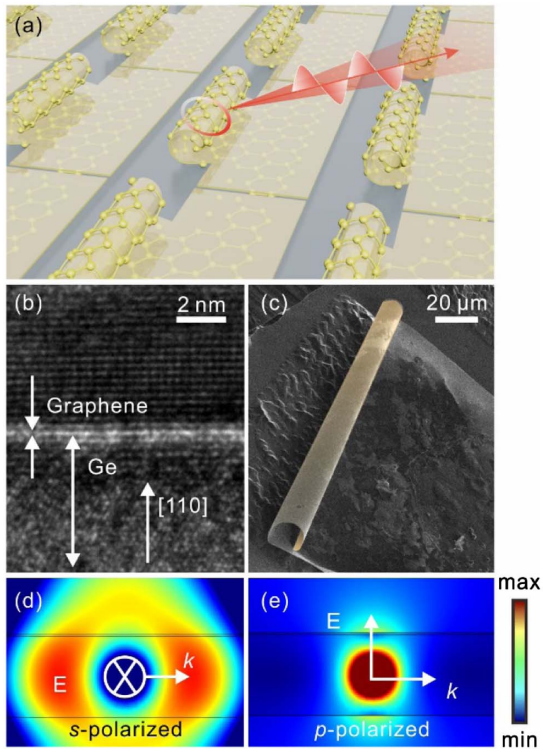

Fig. 8. (a) Schematic of the heterogeneous 2D material microcavities based on the rolled-up technology. (b) Scanning transmission microscopy (STEM) image of the cross section of monolayer graphene on the Ge wafer [125]. (c) SEM image of the rolled-up graphene/oxide microtube [125]. (d) and (e) are the electromagnetic field distributions for the enlarged cross section of graphene/oxide layers with s- and p-polarized incident lights [125].

and realized, as demonstrated through PL measurements [19]. Such a microtube with aligned holes was fabricated based on the mechanical superiority of the diamond layer, as shown in Fig. 7(c). Through the coupling with the nitrogen-vacancy center emission in diamond [22], the PL mapping in Fig. 7(d) further verified the strongly enhanced light confinement and implied its possibility in single-mode lasing at the wavelength of 670 nm. The experimental realization on precisely tuning the subwavelength nanopatterns of the constituent layer confirms the feasibility of the rolled-up technology, which is compatible in the 2D-material–involved technique. The critically designed mesostructure in the rolled-up 2D material microtube may be able to bring a drastic breakthrough in critical light manipulation, indicating its high potential in quantum optical performance.

In summary, rolled-up technology is supposed to be an efficient and controllable method for WGM microcavities with the versatility in both heterogeneous material combination and accurate structural design. As sketched in Fig. 8(a), the rolling method would endow such heterogeneous 2D material microtubular cavities with on-chip, CMOS-compatible, and 3D-integratable properties. Recently, Yin *et al.* demonstrated the graphene-activated optoplasmonic microcavity by transferring the graphene layer onto the rolled-up microtube [124]. While the presence of graphene facilitates an enhanced sensitivity in surface detection, the photodegradation of dye molecules is monitored, paving the way for real-time and high-precision sensors. Meanwhile, graphene/oxide microtubes were constructed based on a CVD-grown monolayer graphene [Fig. 8(b)] with a transfer-free advantage, as shown in Fig. 8(c) [125]. The integration of graphene enables intriguing photonic phenomena, such as polarization-dependent enhancement [46,47], which is further demonstrated through simulation results, as shown in Figs. 8(d) and 8(e). Besides, in-plane strain would be introduced in the graphene layer during the rolling process, which indicates tunable properties towards target performances for the graphene-based microtube as optical devices. Most importantly, since the 3D configuration could support optical resonances, the coupling in graphene-integrated tubular microcavity presents high potential in expanding the optical community with novel applications. Additionally, with the nanoscale thickness tube wall, it would ensure an extremely efficient coupling between the 2D materials and microcavities through the evanescent field. We believe that such hybridized modes in rolled-up microcavities may offer a novel-type platform in lasing, sensing, and light modulating.

6. CONCLUSION

This review summarized recent research regarding the integration of 2D materials and optical WGM microcavities. The nontrivial band structure of graphene enables a series of

appealing phenomena. The heterogeneous graphene microcavities can support hybrid plasmonic WGMs and exhibit ultrahigh sensitive performance. Most importantly, based on the synergy effect of graphene and the WGM microcavity, the heterogeneous structure features a tunable effect, paving the way in light modulation for realistic devices with compact, efficient, broadband, and fast properties. Considering the light confinement of graphene, the advantages of using graphene as both the electrode and the substrate for epitaxial growth further indicate its possible potentials in nanolasers. As another important type of 2D material, TMDCs could boost superior emission, enabling novel light sources in the visible range. Moreover, the emerging of black phosphorus and hBN would broaden the spectral range, realizing the total coverage from ultraviolet to the microwave, possessing possible potentials in nanophotonics. In conclusion, the integration of 2D materials with WGM microcavities could highly enhance the light–matter interaction, thus optimizing the performance of 2D materials towards targeted functional devices, also providing a novel and feasible solution in light control and manipulation.

With the development of information and communication in our daily life, it demands ultrafast and low-loss techniques, which makes the method of using electrons as information carriers no longer qualified. The proposal of "photon circuits," where photons carry and transfer messages, is supposed to be a viable scheme. Therefore, research on integrated circuits with optical devices becomes essential. Meanwhile, the emerging field of 2D materials provides the traditional WGM microcavities with new schemes in light control and light–matter manipulation, implying potential applications in the emitter, modulator, and photodetector.

Funding. National Natural Science Foundation of China (NSFC) (U1632115, 51711540298); Science and Technology Commission of Shanghai Municipality (STCSM) (19XD1400600, 17JC1401700); Key Technologies Research and Development Program (2015ZX02102-003); Changjiang Young Scholars Program of China.

REFERENCES

1. K. J. Vahala, "Optical microcavities," Nature **424**, 839–846 (2003).
2. T. J. Kippenberg, S. M. Spillane, D. K. Armani, and K. J. Vahala, "Fabrication and coupling to planar high-*Q* silica disk microcavities," Appl. Phys. Lett. **83**, 797–799 (2003).
3. D. K. Armani, T. J. Kippenberg, S. M. Spillane, and K. J. Vahala, "Ultra-high-*Q* toroid microcavity on a chip," Nature **421**, 925–928 (2003).
4. L. Ge, L. Feng, and H. G. L. Schwefel, "Optical microcavities: new understandings and developments," Photon. Res. **5**, M1–M3 (2017).
5. Y. Zhi, X. Yu, Q. Gong, L. Yang, and Y. Xiao, "Single nanoparticle detection using optical microcavities," Adv. Mater. **29**, 1604920 (2017).
6. X. Jiang, Y. Xiao, C. Zou, L. He, C. Dong, B. Li, Y. Li, F. Sun, L. Yang, and Q. Gong, "Highly unidirectional emission and ultralow-threshold lasing from on-chip ultrahigh-*Q* microcavities," Adv. Mater. **24**, P260–P264 (2012).
7. W. Chen, J. Zhang, B. Peng, S. K. Özdemir, X. Fan, and L. Yang, "Parity-time-symmetric whispering-gallery mode nanoparticle sensor [invited]," Photon. Res. **6**, A23–A30 (2018).
8. X. Zhang, Q. Cao, Z. Wang, Y. Liu, C. Qiu, L. Yang, Q. Gong, and Y. Xiao, "Symmetry-breaking-induced nonlinear optics at a microcavity surface," Nat. Photonics **13**, 21–24 (2019).
9. Q. Song, "Emerging opportunities for ultra-high *Q* whispering gallery mode microcavities," Sci. China Phys. Mech. Astron. **62**, 074231 (2019).
10. J. R. Buck and H. J. Kimble, "Optimal sizes of dielectric microspheres for cavity QED with strong coupling," Phys. Rev. A **67**, 033806 (2003).
11. V. Zamora, A. Diez, M. V. Andres, and B. Gimeno, "Refractometric sensor based on whispering-gallery modes of thin capillaries," Opt. Express **15**, 12011–12016 (2007).
12. M. G. Senthil, M. N. Petrovich, Y. Jung, J. S. Wilkinson, and M. N. Zervas, "Hollow-bottle optical microresonators," Opt. Express **19**, 20773–20784 (2011).
13. Y. Xiao, S. K. Ozdemir, V. Gaddam, C. Dong, N. Imoto, and L. Yang, "Quantum nondemolition measurement of photon number via optical Kerr effect in an ultra-high-*Q* microtoroid cavity," Opt. Express **16**, 21462–21475 (2008).
14. Q. Song, W. Fang, B. Liu, S. Ho, G. S. Solomon, and H. Cao, "Chaotic microcavity laser with high quality factor and unidirectional output," Phys. Rev. A **80**, 041807 (2009).
15. G. Huang and Y. Mei, "Electromagnetic wave propagation in a rolled-up tubular microcavity," J. Mater. Chem. C **5**, 2758–2770 (2017).
16. J. Wang, T. Zhan, G. Huang, P. K. Chu, and Y. Mei, "Optical microcavities with tubular geometry: properties and applications," Laser Photon. Rev. **8**, 521–547 (2014).
17. J. Wang, T. Zhan, G. Huang, X. Cui, X. Hu, and Y. Mei, "Tubular oxide microcavity with high-index-contrast walls: Mie scattering theory and 3D confinement of resonant modes," Opt. Express **20**, 18555–18567 (2012).
18. C. Strelow, H. Rehberg, C. M. Schultz, H. Welsch, C. Heyn, D. Heitmann, and T. Kipp, "Optical microcavities formed by semiconductor microtubes using a bottlelike geometry," Phys. Rev. Lett. **101**, 127403 (2008).
19. Z. Tian, S. Li, S. Kiravittaya, B. Xu, S. Tang, H. Zhen, W. Lu, and Y. Mei, "Selected and enhanced single whispering-gallery mode emission from a mesostructured nanomembrane microcavity," Nano Lett. **18**, 8035–8040 (2018).
20. X. Lin, Y. Fang, L. Zhu, J. Zhang, G. Huang, J. Wang, and Y. Mei, "Self-rolling of oxide nanomembranes and resonance coupling in tubular optical microcavity," Adv. Opt. Mater. **4**, 936–942 (2016).
21. Y. Li, Y. Fang, J. Wang, L. Wang, S. Tang, C. Jiang, L. Zheng, and Y. Mei, "Integrative optofluidic microcavity with tubular channels and coupled waveguides via two-photon polymerization," Lab Chip **16**, 4406–4414 (2016).
22. Z. Tian, L. Zhang, Y. Fang, B. Xu, S. Tang, N. Hu, Z. An, Z. Chen, and Y. Mei, "Deterministic self-rolling of ultrathin nanocrystalline diamond nanomembranes for 3D tubular/helical architecture," Adv. Mater. **29**, 1604572 (2017).
23. J. Wang, F. Bo, S. Wan, W. Li, F. Gao, J. Li, G. Zhang, and J. Xu, "High-*Q* lithium niobate microdisk resonators on a chip for efficient electro-optic modulation," Opt. Express **23**, 23072–23078 (2015).
24. Z. Gu, K. Wang, W. Sun, J. Li, S. Liu, Q. Song, and S. Xiao, "Two-photon pumped $CH_3NH_3PbBr_3$ perovskite microwire lasers," Adv. Opt. Mater. **4**, 472–479 (2016).
25. A. Autere, H. Jussila, Y. Dai, Y. Wang, H. Lipsanen, and Z. Sun, "Nonlinear optics with 2D layered materials," Adv. Mater. **30**, 1705963 (2018).
26. M. Li, L. Zhang, L. Tong, and D. Dai, "Hybrid silicon nonlinear photonics [invited]," Photon. Res. **6**, B13–B22 (2018).
27. X. Liu, Q. Guo, and J. Qiu, "Emerging low-dimensional materials for nonlinear optics and ultrafast photonics," Adv. Mater. **29**, 1605886 (2017).
28. D. Jariwala, T. J. Marks, and M. C. Hersam, "Mixed-dimensional van der Waals heterostructures," Nat. Mater. **16**, 170–181 (2017).
29. M. Furchi, A. Urich, A. Pospischil, G. Lilley, K. Unterrainer, H. Detz, P. Klang, A. M. Andrews, W. Schrenk, G. Strasser, and T. Mueller, "Microcavity-integrated graphene photodetector," Nano Lett. **12**, 2773–2777 (2012).
30. A. K. Geim and K. S. Novoselov, "The rise of graphene," Nat. Mater. **6**, 183–191 (2007).
31. A. K. Geim, "Graphene: status and prospects," Science **324**, 1530–1534 (2009).

32. C. N. R. Rao, A. K. Sood, K. S. Subrahmanyam, and A. Govindaraj, "Graphene: the new two-dimensional nanomaterial," Angew. Chem. Int. Ed. **48**, 7752–7777 (2009).
33. M. J. Allen, V. C. Tung, and R. B. Kaner, "Honeycomb carbon: a review of graphene," Chem. Rev. **110**, 132–145 (2010).
34. J. Wang, S. Deng, Z. Liu, and Z. Liu, "The rare two-dimensional materials with Dirac cones," Natl. Sci. Rev. **2**, 22–39 (2015).
35. A. A. Balandin, S. Ghosh, W. Bao, I. Calizo, D. Teweldebrhan, F. Miao, and C. N. Lau, "Superior thermal conductivity of single-layer graphene," Nano Lett. **8**, 902–907 (2008).
36. K. S. Novoselov, V. I. Fal'Ko, L. Colombo, P. R. Gellert, M. G. Schwab, and K. Kim, "A roadmap for graphene," Nature **490**, 192–200 (2012).
37. Y. Zhang, Y. Tan, H. L. Stormer, and P. Kim, "Experimental observation of the quantum Hall effect and Berry's phase in graphene," Nature **438**, 201–204 (2005).
38. Z. Sun and H. Chang, "Graphene and graphene-like two-dimensional materials in photodetection: mechanisms and methodology," ACS Nano **8**, 4133–4156 (2014).
39. C. Si, Z. Sun, and F. Liu, "Strain engineering of graphene: a review," Nanoscale **8**, 3207–3217 (2016).
40. D. Zhan, J. Yan, L. Lai, Z. Ni, L. Liu, and Z. Shen, "Engineering the electronic structure of graphene," Adv. Mater. **24**, 4055–4069 (2012).
41. C. Stampfer, J. Guettinger, F. Molitor, D. Graf, T. Ihn, and K. Ensslin, "Tunable Coulomb blockade in nanostructured graphene," Appl. Phys. Lett. **92**, 012102 (2008).
42. X. Gan, K. F. Mak, Y. Gao, Y. You, F. Hatami, J. Hone, T. F. Heinz, and D. Englund, "Strong enhancement of light–matter interaction in graphene coupled to a photonic crystal nanocavity," Nano Lett. **12**, 5626–5631 (2012).
43. P. Wang, O. Liang, W. Zhang, T. Schroeder, and Y. Xie, "Ultra-sensitive graphene-plasmonic hybrid platform for label-free detection," Adv. Mater. **25**, 4918–4924 (2013).
44. Z. Fang, S. Thongrattanasiri, A. Schlather, Z. Liu, L. Ma, Y. Wang, P. M. Ajayan, P. Nordlander, N. J. Halas, and F. J. García De Abajo, "Gated tunability and hybridization of localized plasmons in nanostructured graphene," ACS Nano **7**, 2388–2395 (2013).
45. O. V. Kotov and Y. E. Lozovik, "Cavity plasmon polaritons in monolayer graphene," Phys. Lett. A **375**, 2573–2576 (2011).
46. L. Yu, J. Zheng, Y. Xu, D. Dai, and S. He, "Local and nonlocal optically induced transparency effects in graphene–silicon hybrid nanophotonic integrated circuits," ACS Nano **8**, 11386–11393 (2014).
47. Q. Bao, H. Zhang, B. Wang, Z. Ni, C. H. Y. X. Lim, Y. Wang, D. Y. Tang, and K. P. Loh, "Broadband graphene polarizer," Nat. Photonics **5**, 411–415 (2011).
48. J. Zhao, W. Qiu, Y. Huang, J. Wang, Q. Kan, and J. Pan, "Investigation of plasmonic whispering-gallery mode characteristics for graphene monolayer coated dielectric nanodisks," Opt. Lett. **39**, 5527–5530 (2014).
49. F. Zangeneh-Nejad and R. Safian, "A graphene-based THz ring resonator for label-free sensing," IEEE Sens. J. **16**, 4338–4344 (2016).
50. H. Fan, C. Xia, L. Fan, L. Wang, and M. Shen, "Graphene-supported plasmonic whispering-gallery mode in a metal-coated microcavity for sensing application with ultrahigh sensitivity," Opt. Commun. **410**, 668–673 (2018).
51. X. Zhang, H. Fan, X. Jiang, and M. Xiao, "Controllable coupling of an ultra-high-*Q* microtoroid cavity with monolayer graphene," in *CLEO: Science and Innovations* (Optical Society of America, 2017), paper JTu5A-79.
52. Y. Wu, B. Yao, C. Yu, and Y. Rao, "Optical graphene gas sensors based on microfibers: a review," Sensors **18**, 941 (2018).
53. B. Huang, Z. Li, Z. Liu, G. Zhou, S. Hao, J. Wu, B. Gu, and W. Duan, "Adsorption of gas molecules on graphene nanoribbons and its implication for nanoscale molecule sensor," J. Phys. Chem. C **112**, 13442–13446 (2008).
54. C. Melios, C. E. Giusca, V. Panchal, and O. Kazakova, "Water on graphene: review of recent progress," 2D Mater. **5**, 22001 (2018).
55. B. C. Yao, Y. Wu, A. Q. Zhang, Y. J. Rao, Z. G. Wang, Y. Cheng, Y. Gong, W. L. Zhang, Y. F. Chen, and K. S. Chiane, "Graphene enhanced evanescent field in microfiber multimode interferometer for highly sensitive gas sensing," Opt. Express **22**, 28154–28162 (2014).
56. B. N. Shivananju, W. Yu, Y. Liu, Y. Zhang, B. Lin, S. Li, and Q. Bao, "The roadmap of graphene-based optical biochemical sensors," Adv. Funct. Mater. **27**, 1603918 (2017).
57. Y. Wu, T. Zhang, Y. Rao, and Y. Gong, "Miniature interferometric humidity sensors based on silica/polymer microfiber knot resonators," Sens. Actuators B **155**, 258–263 (2011).
58. C. Yu, Y. Wu, X. Liu, B. Yao, F. Fu, Y. Gong, Y. Rao, and Y. Chen, "Graphene oxide deposited microfiber knot resonator for gas sensing," Opt. Mater. Express **6**, 727–733 (2016).
59. B. Yao, C. Yu, Y. Wu, S. Huang, H. Wu, Y. Gong, Y. Chen, Y. Li, C. W. Wong, X. Fan, and Y. Rao, "Graphene-enhanced Brillouin optomechanical microresonator for ultrasensitive gas detection," Nano Lett. **17**, 4996–5002 (2017).
60. A. Madani, S. M. Harazim, V. A. Bolanos Quinones, M. Kleinert, A. Finn, E. S. G. Naz, L. Ma, and O. G. Schmidt, "Optical microtube cavities monolithically integrated on photonic chips for optofluidic sensing," Opt. Lett. **42**, 486–489 (2017).
61. U. Bog, F. Brinkmann, H. Kalt, C. Koos, T. Mappes, M. Hirtz, H. Fuchs, and S. K. Ber, "Large-scale parallel surface functionalization of goblet-type whispering gallery mode microcavity arrays for biosensing applications," Small **10**, 3863–3868 (2014).
62. B. Yao, Y. Liu, S. Huang, C. Choi, Z. Xie, J. F. Flores, Y. Wu, M. Yu, D. Kwong, Y. Huang, Y. Rao, X. Duan, and C. W. Wong, "Broadband gate-tunable terahertz plasmons in graphene heterostructures," Nat. Photonics **12**, 22–28 (2018).
63. M. Liu, X. Yin, E. Ulin-Avila, B. Geng, T. Zentgraf, L. Ju, F. Wang, and X. Zhang, "A graphene-based broadband optical modulator," Nature **474**, 64–67 (2011).
64. M. Midrio, S. Boscolo, M. Moresco, M. Romagnoli, C. De Angelis, A. Locatelli, and A. Capobianco, "Graphene-assisted critically-coupled optical ring modulator," Opt. Express **20**, 23144–23155 (2012).
65. C. T. Phare, Y. Daniel Lee, J. Cardenas, and M. Lipson, "Graphene electro-optic modulator with 30 GHz bandwidth," Nat. Photonics **9**, 511–514 (2015).
66. Z. Wu, Y. Chen, T. Zhang, Z. Shao, Y. Wen, P. Xu, Y. Zhang, and S. Yu, "Design and optimization of optical modulators based on graphene-on-silicon nitride microring resonators," J. Opt. **19**, 045801 (2017).
67. S. Gan, C. Cheng, Y. Zhan, B. Huang, X. Gan, S. Li, S. Lin, X. Li, J. Zhao, H. Chen, and Q. Bao, "A highly efficient thermo-optic microring modulator assisted by graphene," Nanoscale **7**, 2249–2255 (2015).
68. S. Yu, X. Wu, K. Chen, B. Chen, X. Guo, D. Dai, L. Tong, W. Liu, and Y. R. Shen, "All-optical graphene modulator based on optical Kerr phase shift," Optica **3**, 541–544 (2016).
69. K. Wu, Y. Wang, C. Qiu, and J. Chen, "Thermo-optic all-optical devices based on two-dimensional materials," Photon. Res. **6**, C22 (2018).
70. C. Qiu, Y. Yang, C. Li, Y. Wang, K. Wu, and J. Chen, "All-optical control of light on a graphene-on-silicon nitride chip using thermo-optic effect," Sci. Rep. **7**, 17046 (2017).
71. M. Mohsin, D. Schall, M. Otto, B. Chmielak, S. Suckow, and D. Neumaier, "Towards the predicted high performance of waveguide integrated electro-refractive phase modulators based on graphene," IEEE Photon. J. **9**, 7800507 (2017).
72. C. Qiu, W. Gao, R. Vajtai, P. M. Ajayan, J. Kono, and Q. Xu, "Efficient modulation of 1.55 μm radiation with gated graphene on a silicon microring resonator," Nano Lett. **14**, 6811–6815 (2014).
73. Y. Ding, X. Zhu, S. Xiao, H. Hu, L. H. Frandsen, N. A. Mortensen, and K. Yvind, "Effective electro-optical modulation with high extinction ratio by a graphene–silicon microring resonator," Nano Lett. **15**, 4393–4400 (2015).
74. Y. Gao, W. Zhou, X. Sun, H. K. Tsang, and C. Shu, "Cavity-enhanced thermo-optic bistability and hysteresis in a graphene-on-Si_3N_4 ring resonator," Opt. Lett. **42**, 1950–1953 (2017).
75. Y. Wang, C. Xue, Z. Zhang, H. Zheng, W. Zhang, and S. Yan, "Tunable optical analog to electromagnetically induced transparency in graphene-ring resonators system," Sci. Rep. **6**, 38891 (2016).
76. B. Yao, S. W. Huang, Y. Liu, A. K. Vinod, C. Choi, M. Hoff, Y. Li, M. Yu, Z. Feng, D. L. Kwong, Y. Huang, Y. Rao, X. Duan, and C. W. Wong, "Gate-tunable frequency combs in graphene-nitride microresonators," Nature **558**, 410–414 (2018).

77. A. Villois and D. V. Skryabin, "Soliton and quasi-soliton frequency combs due to second harmonic generation in microresonators," Opt. Express **27**, 7098–7107 (2019).
78. M. Jiang, J. Li, C. Xu, S. Wang, C. Shan, B. Xuan, Y. Ning, and D. Shen, "Graphene induced high-Q hybridized plasmonic whispering gallery mode microcavities," Opt. Express **22**, 23836–23850 (2014).
79. J. Li, M. Jiang, C. Xu, Y. Wang, Y. Lin, J. Lu, and Z. Shi, "Plasmon coupled Fabry–Perot lasing enhancement in graphene/ZnO hybrid microcavity," Sci. Rep. **5**, 9263 (2015).
80. J. Li, C. Xu, H. Nan, M. Jiang, G. Gao, Y. Lin, J. Dai, G. Zhu, Z. Ni, S. Wang, and Y. Li, "Graphene surface plasmon induced optical field confinement and lasing enhancement in ZnO whispering-gallery microcavity," ACS Appl. Mater. Interfaces **6**, 10469–10475 (2014).
81. J. Li, Y. Lin, J. Lu, C. Xu, Y. Wang, Z. Shi, and J. Dai, "Single mode ZnO whispering-gallery submicron cavity and graphene improved lasing performance," ACS Nano **9**, 6794–6800 (2015).
82. C. Xu, F. Qin, Q. Zhu, J. Lu, Y. Wang, J. Li, Y. Lin, Q. Cui, Z. Shi, and A. G. Manohari, "Plasmon-enhanced ZnO whispering-gallery mode lasing," Nano Res. **11**, 3050–3064 (2018).
83. H. Baek, C. Lee, K. Chung, and G. Yi, "Epitaxial GaN microdisk lasers grown on graphene microdots," Nano Lett. **13**, 2782–2785 (2013).
84. K. Chung, H. Yoo, J. K. Hyun, H. Oh, Y. Tchoe, K. Lee, H. Baek, M. Kim, and G. Yi, "Flexible GaN light-emitting diodes using GaN microdisks epitaxial laterally overgrown on graphene dots," Adv. Mater. **28**, 7688–7694 (2016).
85. J. Zheng, H. Xu, J. J. Wang, S. Winters, C. Motta, E. Karademir, W. Zhu, E. Varrla, G. S. Duesberg, S. Sanvito, W. Hu, and J. F. Donegan, "Vertical single-crystalline organic nanowires on graphene: solution-phase epitaxy and optical microcavities," Nano Lett. **16**, 4754–4762 (2016).
86. Y. Kim, S. Kwon, J. M. Lee, M. Hwang, J. Kang, W. I. Park, and H. Park, "Graphene-contact electrically driven microdisk lasers," Nat. Commun. **3**, 1123 (2012).
87. F. Xia, H. Wang, D. Xiao, M. Dubey, and A. Ramasubramaniam, "Two-dimensional material nanophotonics," Nat. Photonics **8**, 899–907 (2014).
88. Q. Hao, J. Pang, Y. Zhang, J. Wang, L. Ma, and O. G. Schmidt, "Boosting the photoluminescence of monolayer MoS_2 on high-density nanodimer arrays with sub-10 nm gap," Adv. Opt. Mater. **6**, 1700984 (2018).
89. G. Wang, X. Marie, I. Gerber, T. Amand, D. Lagarde, L. Bouet, M. Vidal, A. Balocchi, and B. Urbaszek, "Giant enhancement of the optical second-harmonic emission of WSe_2 monolayers by laser excitation at exciton resonances," Phys. Rev. Lett. **114**, 097403 (2015).
90. A. Ramasubramaniam, "Large excitonic effects in monolayers of molybdenum and tungsten dichalcogenides," Phys. Rev. B **86**, 115409 (2012).
91. A. Chernikov, T. C. Berkelbach, H. M. Hill, A. Rigosi, Y. Li, O. B. Aslan, D. R. Reichman, M. S. Hybertsen, and T. F. Heinz, "Exciton binding energy and nonhydrogenic Rydberg series in monolayer WS_2," Phys. Rev. Lett. **113**, 076802 (2014).
92. C. Janisch, H. Song, C. Zhou, Z. Lin, A. L. Elías, D. Ji, M. Terrones, Q. Gan, and Z. Liu, "MoS_2 monolayers on nanocavities: enhancement in light–matter interaction," 2D Mater. **3**, 025017 (2016).
93. K. F. Mak, C. Lee, J. Hone, J. Shan, and T. F. Heinz, "Atomically thin MoS_2: a new direct-gap semiconductor," Phys. Rev. Lett. **105**, 136805 (2010).
94. K. F. Mak and J. Shan, "Photonics and optoelectronics of 2D semiconductor transition metal dichalcogenides," Nat. Photonics **10**, 216–226 (2016).
95. R. I. Woodward, R. C. T. Howe, G. Hu, F. Torrisi, M. Zhang, T. Hasan, and E. J. R. Kelleher, "Few-layer MoS_2 saturable absorbers for short-pulse laser technology: current status and future perspectives [invited]," Photon. Res. **3**, A30–A42 (2015).
96. J. Liu, T. Wang, X. Li, and N. Liu, "Enhanced absorption of monolayer MoS_2 with resonant back reflector," J. Appl. Phys. **115**, 193511 (2014).
97. S. Dufferwiel, S. Schwarz, F. Withers, A. A. P. Trichet, F. Li, M. Sich, O. Del Pozo-Zamudio, C. Clark, A. Nalitov, D. D. Solnyshkov, G. Malpuech, K. S. Novoselov, J. M. Smith, M. S. Skolnick, D. N. Krizhanovskii, and A. I. Tartakovskii, "Exciton–polaritons in van der Waals heterostructures embedded in tunable microcavities," Nat. Commun. **6**, 8579 (2015).
98. L. Reeves, Y. Wang, and T. F. Krauss, "2D material microcavity light emitters: to lase or not to lase?" Adv. Opt. Mater. **6**, 1800272 (2018).
99. T. Fryett, A. Zhan, and A. Majumdar, "Cavity nonlinear optics with layered materials," Nanophotonics **7**, 355–370 (2017).
100. J. C. Reed, A. Y. Zhu, H. Zhu, F. Yi, and E. Cubukcu, "Wavelength tunable microdisk cavity light source with a chemically enhanced MoS_2 emitter," Nano Lett. **15**, 1967–1971 (2015).
101. S. Wu, S. Buckley, J. R. Schaibley, L. Feng, J. Yan, D. G. Mandrus, F. Hatami, W. Yao, J. Vučković, A. Majumdar, and X. Xu, "Monolayer semiconductor nanocavity lasers with ultralow thresholds," Nature **520**, 69–72 (2015).
102. Y. Ye, Z. J. Wong, X. Lu, X. Ni, H. Zhu, X. Chen, Y. Wang, and X. Zhang, "Monolayer excitonic laser," Nat. Photonics **9**, 733–737 (2015).
103. O. Salehzadeh, M. Djavid, N. H. Tran, I. Shih, and Z. Mi, "Optically pumped two-dimensional MoS_2 lasers operating at room-temperature," Nano Lett. **15**, 5302–5306 (2015).
104. C. Javerzac-Galy, A. Kumar, R. D. Schilling, N. Piro, S. Khorasani, M. Barbone, I. Goykhman, J. B. Khurgin, A. C. Ferrari, and T. J. Kippenberg, "Excitonic emission of monolayer semiconductors near-field coupled to high-Q microresonators," Nano Lett. **18**, 3138–3146 (2018).
105. R. Maiti, R. A. Hemnani, R. Amin, Z. Ma, M. H. Tahersima, T. A. Empante, H. Dalir, R. Agarwal, L. Bartels, and V. J. Sorger, "A semi-empirical integrated microring cavity approach for 2D material optical index identification at 1.55 μm," Nanophotonics **8**, 435–441 (2019).
106. J. C. Reed, S. C. Malek, F. Yi, C. H. Naylor, A. T. C. Johnson, and E. Cubukcu, "Photothermal characterization of MoS_2 emission coupled to a microdisk cavity," Appl. Phys. Lett. **109**, 193109 (2016).
107. Y. Mi, Z. Zhang, L. Zhao, S. Zhang, J. Chen, Q. Ji, J. Shi, X. Zhou, R. Wang, J. Shi, W. Du, Z. Wu, X. Qiu, Q. Zhang, Y. Zhang, and X. Liu, "Tuning excitonic properties of monolayer MoS_2 with microsphere cavity by high-throughput chemical vapor deposition method," Small **13**, 1701694 (2017).
108. B. W. H. Baugher, H. O. H. Churchill, Y. Yang, and P. Jarillo-Herrero, "Optoelectronic devices based on electrically tunable p–n diodes in a monolayer dichalcogenide," Nat. Nanotechnol. **9**, 262–267 (2014).
109. D. R. Kazanov, A. V. Poshakinskiy, V. Y. Davydov, A. N. Smirnov, I. A. Eliseyev, D. A. Kirilenko, M. Remškar, S. Fathipour, A. Mintairov, A. Seabaugh, B. Gil, and T. V. Shubina, "Multiwall MoS_2 tubes as optical resonators," Appl. Phys. Lett. **113**, 101106 (2018).
110. L. Britnell, R. M. Ribeiro, A. Eckmann, R. Jalil, B. D. Belle, A. Mishchenko, Y.-J. Kim, R. V. Gorbachev, T. Georgiou, S. V. Morozov, A. N. Grigorenko, A. K. Geim, C. Casiraghi, A. H. Castro Neto, and K. S. Novoselov, "Strong light-matter interactions in heterostructures of atomically thin films," Science **340**, 1311–1314 (2013).
111. T. Ren, P. Song, J. Chen, and K. P. Loh, "Whisper gallery modes in monolayer tungsten disulfide-hexagonal boron nitride optical cavity," ACS Photon. **5**, 353–358 (2017).
112. C. Lee, G. Lee, A. M. van der Zande, W. Chen, Y. Li, M. Han, X. Cui, G. Arefe, C. Nuckolls, T. F. Heinz, J. Guo, J. Hone, and P. Kim, "Atomically thin p–n junctions with van der Waals heterointerfaces," Nat. Nanotechnol. **9**, 676–681 (2014).
113. X. Hong, J. Kim, S. Shi, Y. Zhang, C. Jin, Y. Sun, S. Tongay, J. Wu, Y. Zhang, and F. Wang, "Ultrafast charge transfer in atomically thin MoS_2/WS_2 heterostructures," Nat. Nanotechnol. **9**, 682–686 (2014).
114. P. K. Shandilya, J. E. Fröch, M. Mitchell, D. P. Lake, S. Kim, M. Toth, B. Behera, C. Healey, I. Aharonovich, and P. E. Barclay, "Hexagonal boron nitride cavity optomechanics," Nano Lett. **19**, 1343–1350 (2019).
115. L. Li, Y. Yu, G. J. Ye, Q. Ge, X. Ou, H. Wu, D. Feng, X. H. Chen, and Y. Zhang, "Black phosphorus field-effect transistors," Nat. Nanotechnol. **9**, 372–377 (2014).
116. Z. Wang, H. Jia, X. Zheng, R. Yang, Z. Wang, G. J. Ye, X. H. Chen, J. Shan, and P. X. L. Feng, "Black phosphorus nanoelectromechanical resonators vibrating at very high frequencies," Nanoscale **7**, 877–884 (2015).

117. Y. Chen, G. Jiang, S. Chen, Z. Guo, X. Yu, C. Zhao, H. Zhang, Q. Bao, S. Wen, D. Tang, and D. Fan, "Mechanically exfoliated black phosphorus as a new saturable absorber for both *Q*-switching and mode-locking laser operation," Opt. Express **23**, 12823–12833 (2015).
118. F. Xia, H. Wang, and Y. Jia, "Rediscovering black phosphorus as an anisotropic layered material for optoelectronics and electronics," Nat. Commun. **5**, 4458 (2014).
119. S. Schwaiger, M. Broell, A. Krohn, A. Stemmann, C. Heyn, Y. Stark, D. Stickler, D. Heitmann, and S. Mendach, "Rolled-up three-dimensional metamaterials with a tunable plasma frequency in the visible regime," Phys. Rev. Lett. **102**, 163903 (2009).
120. Y. Yin, S. L. Li, S. Giudicatti, C. Y. Jiang, L. B. Ma, and O. G. Schmidt, "Strongly hybridized plasmon-photon modes in optoplasmonic microtubular cavities," Phys. Rev. B **92**, 241403 (2015).
121. Y. Yin, S. Li, S. Boettner, F. Yuan, S. Giudicatti, E. S. G. Naz, L. Ma, and O. G. Schmidt, "Localized surface plasmons selectively coupled to resonant light in tubular microcavities," Phys. Rev. Lett. **116**, 253904 (2016).
122. Y. Yin, S. Li, V. Engemaier, S. Giudicatti, E. S. G. Naz, L. Ma, and O. G. Schmidt, "Hybridization of photon-plasmon modes in metal-coated microtubular cavities," Phys. Rev. A **94**, 013832 (2016).
123. Y. Yin, Y. Chen, E. S. G. Naz, X. Lu, S. Li, V. Engemaier, L. Ma, and O. G. Schmidt, "Silver nanocap enabled conversion and tuning of hybrid photon-plasmon modes in microtubular cavities," ACS Photon. **4**, 736–740 (2017).
124. Y. Yin, J. Pang, J. Wang, X. Lu, Q. Hao, E. Saei Ghareh Naz, X. Zhou, L. Ma, and O. G. Schmidt, "Graphene-activated optoplasmonic nanomembrane cavities for photodegradation detection," ACS Appl. Mater. Interfaces **11**, 15891–15897 (2019).
125. L. Wang, Z. Tian, B. Zhang, B. Xu, T. Wang, Y. Wang, S. Li, Z. Di, and Y. Mei, "On-chip rolling design for controllable strain engineering and enhanced photon–phonon interaction in graphene," Small **15**, 1805477 (2019).